An Experimental Study of Deformation of a Columnar Dendritic Mushy Zone Using a Transparent Succinonitrile-Acetone Alloy

H.F. SHEN and C. BECKERMANN

The deformation of a directionally solidified columnar dendritic mushy zone in a transparent succinonitrile-acetone (SCN-ACE) alloy has been studied experimentally. In addition to solidifying dendritically like a metal alloy, this alloy also has mechanical properties that are similar to those of metals near the melting point. The experiments are relevant, for example, to the deformation of a partially solidified strand during continuous casting of steel slabs. A test cell was designed which allows for directional solidification of the alloy and controlled compression of the solid-liquid mush which forms. Measurements during solidification and deformation include temperatures, interface positions, local displacements of the solid skeleton in the mush, and liquid concentrations. Results are presented for a range of initial test-cell thicknesses, deformation amounts, and deformation start times. The measurements are suitable for validation of future models.

I. INTRODUCTION

DEFORMATION of the solid skeleton in the mushy zone during solidification of alloys is an important phenomenon in many casting processes, including continuous casting of various steel shapes, twin-roll casting of thin strips, squeeze casting, semisolid forming, and others.[1–6] If uncontrolled, such deformation of the solid can cause severe macrosegregation defects, in addition to those caused by interdendritic fluid flow.[7] On the other hand, controlled deformation of the mushy zone during solidification, by application of pressure or distributed external forces on the solid shell, can be used to eliminate macrosegregation and shrinkage defects in cast products. The rheological or stress-strain behavior of mushy zones, as well as the mass, momentum, heat, and species transport phenomena occurring during deformation, are not well understood. This study proposes the use of a transparent model system, namely a succinonitrile-acetone (SCN-ACE) alloy, to investigate these issues experimentally.

The present study is primarily motivated by the desire to model and, ultimately, help alleviate the positive centerline macrosegregation commonly observed in continuous casting of steel. In this process, the solid deforms due to bulging between pairs of support rolls and thermal stresses (*e.g.*, due to contractions upon cooling and solidification). The deformation draws enriched liquid into the center of the slab, where it then freezes and causes positive macrosegregation. Miyazawa and Schwerdtfeger[8] developed an early model of macrosegregation due to bulging and solidification shrinkage in continuously cast steel slabs. Between pairs of support rolls, where the strand bulges, the dendrites are assumed to move with the same velocity as the solid shell. In the region where the strand is squeezed together (*i.e.*, at each pair of support rolls), the solid phase is assumed to move with a horizontal velocity which depends linearly on the solid fraction. Lesoult and Sella[9] and El-Bealy and Fredriksson[10] developed solute redistribution equations that account for changes in the volume of a mush element due to interdendritic strains and deformation of the solid skeleton. By focusing solely on thermal strains due to differential contractions in a slab during casting, they were able to explain measured macrosegregation patterns in steel slabs. The most advanced model to date of deformation-induced macrosegregation in the continuous casting of steel was presented very recently by Kajitani *et al.*[11] Based on two-dimensional heat-flow calculations, the bulging of the slab between pairs of support rolls was first simulated using the finite-element code ABAQUS, while neglecting thermal strains. The velocities of the solid skeleton across the deforming mushy zone were then obtained by using the resulting bulging profile of the solid shell and assuming a linear variation of the transverse solid velocity between the solidus isotherm and the centerline in the compression areas. The solute-conservation equation, Darcy's law, and a mass-conservation equation that accounts for shrinkage were solved together iteratively. Although no direct comparisons with experiments are offered, the model produces realistic positive centerline segregation values. Detailed results are presented which allow for an assessment of the various contributions to centerline segregation by bulging, shrinkage, and soft reduction. It is noted that improved descriptions are needed for the deformation behavior of the solid skeleton in the mushy zone, particularly when the solid fraction is high and coherency is increased by coalescence of neighboring columnar dendrite branches.

A variety of techniques have been proposed to alleviate centerline segregation in continuous casting. In soft reduction (SR), compression of the solidifying slab prevents enriched liquid from being drawn down into the solidifying strand by solidification contraction.[12,13,14] In the continuous forging process (or hard reduction (HR)), the slab thickness is reduced during the final stage of solidification.[15,16,17]

H.F. SHEN, formerly Postdoctoral Researcher, Department of Mechanical Engineering, University of Iowa, is Associate Professor, Department of Mechanical Engineering, Tsinghua University, Beijing 100084, People's Republic of China. C. BECKERMANN, Professor, is with the Department of Mechanical and Industrial Engineering, University of Iowa, Iowa City, IA 52242-1527.

Manuscript submitted January 25, 2001.

This method not only solves the problem of centerline segregation and porosity defects, but also makes it possible to select the concentrations in the center in response to product quality requirements. Similar controlled deformation of the mushy zone during solidification is also important in thin-slab casting, continuous strip casting, thin-strip casting, and continuous rolling.[1,2,3]

Alloys of SCN and ACE have been used in the past as transparent analogue materials to study the solidification of metal alloys.[18,19] The SCN-ACE alloys have convenient liquidus temperatures around room temperature, SCN has a low entropy of melting and exhibits bcc plastically crystalline behavior prior to melting, and the thermophysical properties of SCN-ACE alloys are well established.[18,19,20] Not only do such alloys allow for direct observation of typical dendritic solidification processes, but their mechanical behavior is also similar to that of metal alloys just below the melting point. For example, in order to investigate the creep of metal-matrix composites near the melting point, Jones and co-workers[21–24] used SCN and SCN-Al particle-hardened systems to determine the relevant constants in the power law used to model creep behavior.

The objective of the present work is to explore the use of SCN-ACE alloys in experiments to study mushy-zone deformation during solidification. A test cell is constructed to mimic deformation in continuous casting of steel slabs. For the first time, the deformation of the solid skeleton in the mush is directly observed and measured. In addition, local liquid concentrations are measured before and after deformation, in order to understand and quantify the effects of deformation on melt flow and solute redistribution. Numerous temperatures, as well as the location and shape of the mush/liquid interface, are recorded throughout the tests in order to allow for future modeling of the experiments. Measurements are reported for experiments performed by varying the following parameters: initial section thickness before deformation, deformation amount, deformation start time, and deformation speed. It is emphasized that the present study focuses solely on transport phenomena during solidification and deformation. The rheological or stress-strain behavior of SCN-ACE alloy mushy zones should be determined in separate, specially designed experiments. Consequently, no forces were measured in the present study.

II. EXPERIMENTS

Succinonitrile (99 pct pure) and acetone (99.7 pct pure) were used to prepare alloys with solute concentrations of approximately 10+/−1 wt pct acetone. The SCN-ACE phase diagram has approximately linear solidus and liquidus lines, with a liquidus slope of −2.8 K/wt pct and a partition coefficient of 0.1.[18,19] The melting point of pure SCN is 58.081 °C. Hence, the alloys used in the present experiments had liquidus temperatures of around 30 °C. Figure 1(a) shows a schematic of the experimental setup, and Figure 1(b) provides the temperature and concentration measurement locations. The closed test cell, with inner dimensions of 210 mm in height, 150 mm in width, and a variable thickness (from 25 to 45 mm), was constructed using a high-thermal-conductivity copper heat exchanger on one side and low-thermal-conductivity acrylic glass and phenolic plates on the other sides. The heat exchanger was connected to two constant-temperature circulators with a high temperature of

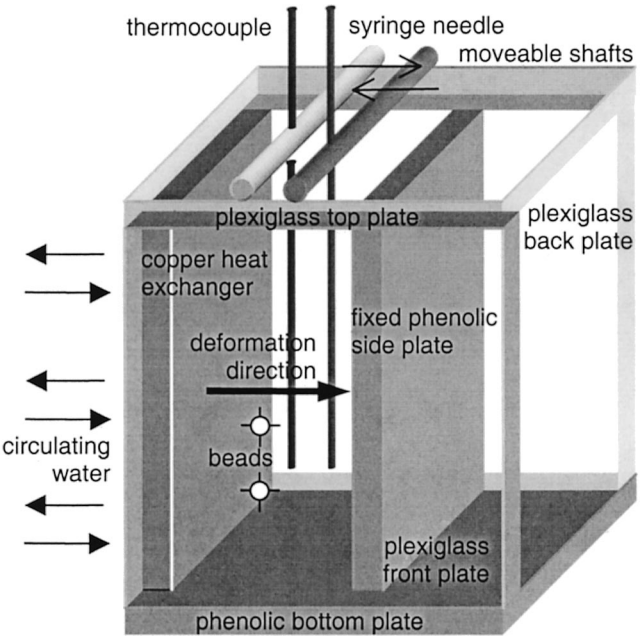

(*a*)

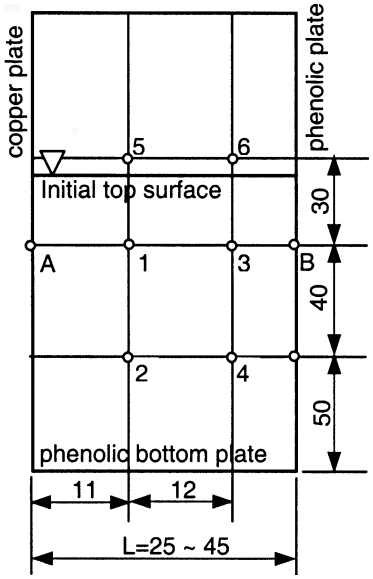

(*b*)

Fig. 1—Experimental setup: (*a*) schematic of the test cell and (*b*) locations of the temperature and liquid concentration measurement positions (all dimensions are in millimeters).

about 50 °C and a low temperature of 0 °C. By controlling the flow rates through three separate chambers inside the heat exchanger, it was possible to achieve accurate isothermality of the heat-exchanger surface. The thermocouple rakes, as well as the syringe needles for the concentration measurements, were inserted from the top of the test cell along the vertical centerline at midwidth. As shown in Figure 1(b), thermocouples A and B were mounted on the heat exchanger and the opposing fixed phenolic side plate, respectively, at a height of 90 mm. Measurement locations 1, 2, and 5 are located 11 mm from the heat exchanger at heights of 50, 90, and 120 mm, respectively. Measurement locations 3, 4, and 6 are located 23 mm from the heat exchanger at

the same three heights. Since the SCN-ACE alloy was poured into the test cell to an initial height of only 110 mm, measurement locations 5 and 6 in Figure 1(b) were only immersed in the alloy after deformation. Before deformation, the thermocouples at those two locations measured the atmospheric temperature inside the test cell just above the free surface. In order to trace the deformation behavior of the solid skeleton in the mush, two rows of black plastic beads with a diameter of 1 mm and a density near that of the SCN-ACE alloy were inserted at heights of about 50 and 90 mm in the test cell near the front wall. The beads were frozen into the solid such that they moved with the same velocity as the solid at that location during deformation. The entire test cell was enclosed in an environmental chamber which was kept close to the mean temperature of the test cell during the tests.

After a uniform and steady temperature of $45+/-5$ °C was attained in the test cell, cooling was initiated by turning a valve on the heat exchanger from the hot to the cold circulator. Soon thereafter, solidification proceeded in an approximately unidirectional fashion from the heat-exchanger surface toward the opposing phenolic side plate. The interface between the mushy zone and the single-phase liquid region (at the location of the primary dendrite tips, hereafter referred to as the mush/liquid interface) at a given height was very uniform in the width direction at all times, indicating that heat losses from the back and front plexiglass walls in Figure 1(a) were negligible. Deformation in the horizontal direction was applied after the SCN-ACE alloy in the test cell was in a mushy state. In the deformation process, the heat exchanger, together with the phenolic bottom plate and the acrylic glass top, back, and front plates, was moved toward the fixed phenolic plate opposing the heat exchanger using a manual spindle mechanism. The fixed phenolic plate, on the right-hand side in Figure 1, can be thought of as the centerline in the thickness direction of a continuously cast steel slab. The thermocouples and syringe needles were fixed in two shafts that moved along with the top plexiglass plate during deformation. In this way, the relative movement of the thermocouples and syringe needles with respect to the solid skeleton during the deformation process was minimized.

The experimental parameters varied were the initial thickness of the test cell (L), the deformation amount (D), the deformation start time (t_S), and the duration of the deformation (t_D) (or, equivalently, the deformation speed, $V = D/t_D$). The deformation start time was measured relative to the start of cooling. Temperatures were recorded at 10-second intervals, with an accuracy of about ± 0.1 °C. To measure the solute concentration of the liquid (C) at various locations in the test cell, small samples (about 2 mL) of liquid were withdrawn with the syringes just before and after deformation. The time elapsed between extruding the samples before and after deformation was about 5 minutes. The samples were analyzed after the completion of each test by measuring their liquidus temperatures. This was accomplished by slowly raising the temperature of a sample until the last solid disappeared.[20] The liquidus temperature was then converted to a concentration using the equation for the liquidus line of the SCN-ACE phase diagram (with a liquidus slope of -2.8 K/wt pct). The liquid concentration was then normalized by the initial concentration C_0, measured by withdrawing a sample from the test cell before initiation of cooling. Only these relative ACE concentrations (C/C_0) are reported here. The mush/liquid interface contours and the deformation process were observed using a video camera through the transparent acrylic glass wall and were analyzed using digital imaging.

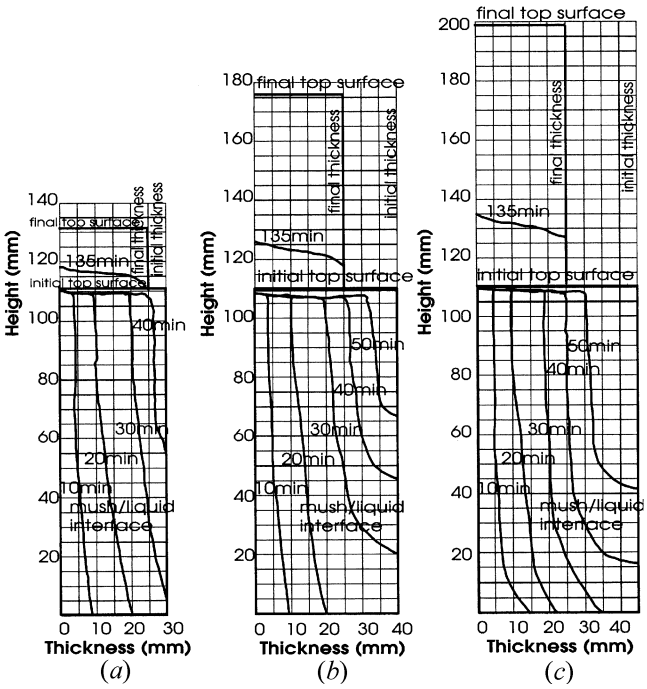

Fig. 2—Development of the mush/liquid interface before and after deformation ($t_S \approx 135$ min, $V = 0.5$ mm/s): (*a*) $L = 30$ mm, $D = 5$ mm; (*b*) $L = 40$ mm, $D = 15$ mm; and (*c*) $L = 45$ mm and $D = 20$ mm.

III. RESULTS AND DISCUSSION

A. *Influence of Deformation Amount for the Same Final Thickness*

Three experiments were performed where the deformation amounts were 5, 15, and 20 mm, while the final thickness of the test cell after deformation was held constant at 25 mm. Hence, the initial test cell thicknesses were 30, 40, and 45 mm in the three tests. In all three tests, the deformation start time was about 135 minutes, and the deformation speed was 0.5 mm/s.

Figures 2(a) through (c) show the measured mush/liquid interface positions for the three tests. Before the mush/liquid interface reaches the fixed phenolic plate on the right-hand side, it develops in approximately the same manner in all tests. The mush/liquid interface is inclined upward, with a larger mush thickness at the bottom. This is caused primarily by natural convection in the melt during solidification, which results in cooling of the melt as it flows downward along the mush/liquid interface. In addition, some free dendrite fragments were observed to settle to the bottom of the test cell during the latter stages of solidification. These fragments presumably originated from the columnar dendrites growing from the cold wall. However, this effect only contributes to the increased thickness of the mushy zone at the bottom in a minor way. Other than for the few equiaxed grains originating from the dendrite fragments, the grain structure was

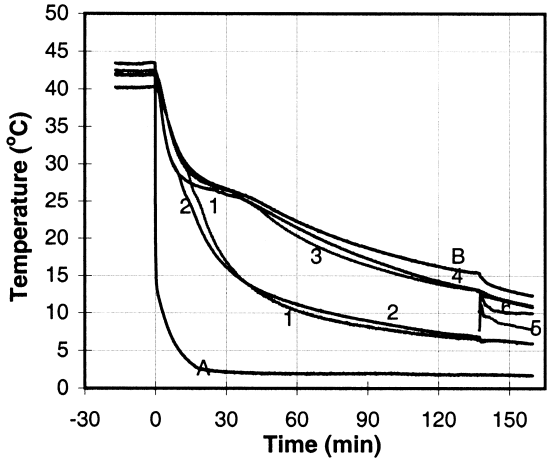

(*a*)

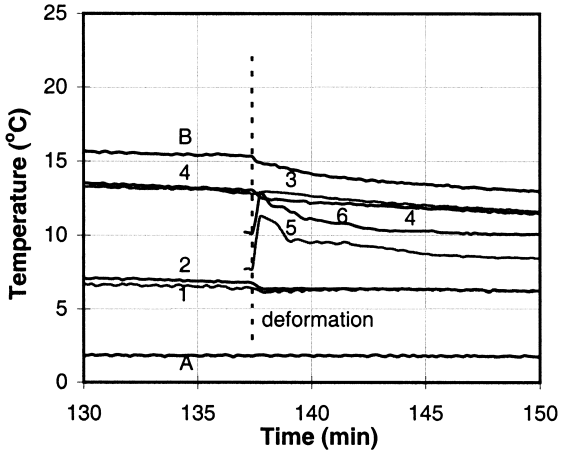

(*b*)

Fig. 3—Temperatures measured during the test with $L = 30$ mm and $D = 5$ mm ($t_S \approx 135$ min, $V = 0.5$ mm/s): (*a*) overall temperature variation and (*b*) close-up of the temperature variation near the deformation time (the vertical dashed line indicates the start of deformation).

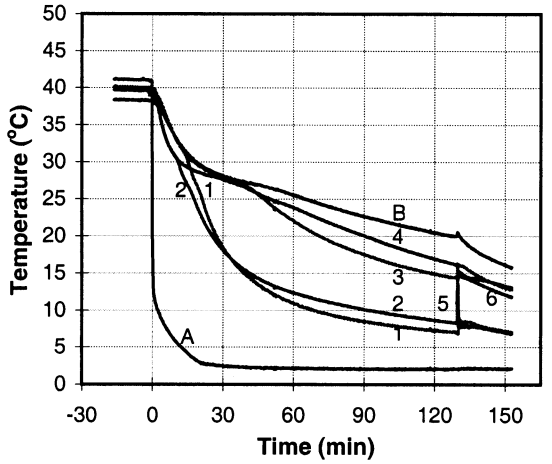

(*a*)

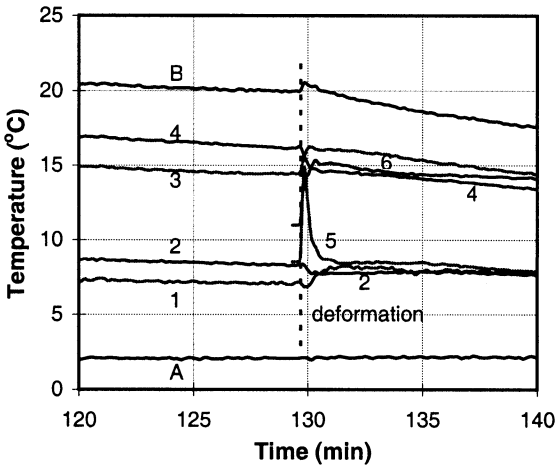

(*b*)

Fig. 4—Temperatures measured during the test with $L = 45$ mm and $D = 20$ mm ($t_S \approx 135$ min, $V = 0.5$ mm/s): (*a*) overall temperature variation and (*b*) close-up of the temperature variation near the deformation time (the vertical dashed line indicates the start of deformation).

columnar. After about 50 minutes, the cooling and solidification rates decrease significantly for the two larger initial test-cell thicknesses. The times when virtually the entire test cell is filled with mush are 80 and 100 minutes for the initial thicknesses of 40 and 45 mm, respectively. After deformation (at $t_S = 135$ min), the height of the free surface in the test cell is increased in accordance with mass conservation. It can be seen from Figure 2 that the region between the initial and final top surface is mostly occupied by liquid expelled from the mush during deformation; however, the lower part is occupied by mush. The upper mush/liquid interface rose by about 5, 15, and 20 mm for the deformation amounts of 5, 15, and 20 mm, respectively, implying that the compression of the mush resulted in some upward movement of solid. The upper mush/liquid interface after deformation is inclined with a larger height adjacent to the heat-exchanger wall, again indicating nonuniform deformation of the solid skeleton.

Figures 3 and 4 show the temperatures measured during the tests with initial thicknesses of 30 and 45 mm, respectively. In the test with an initial thickness of 40 mm, the temperature variations are similar to the ones for 45 mm, except that they are generally a little lower. Initially, the melt temperatures decrease in a fairly uniform fashion until the liquidus temperature is reached, indicating that natural convection produces mixing in the liquid. During solidification, a temperature gradient is established across the thickness of the test cell, while there is comparably little temperature variation in the vertical direction. The temperatures in those parts of the test cell that are still liquid remain close to the liquidus temperature. As expected, the local cooling rates decrease with increasing initial test-cell thickness. For example, just before deformation (approximately 130 minutes into the test), the temperature at location 4 is about 3 °C higher for the larger initial thickness.

The temperature variations directly before and after deformation are better seen in the enlarged plots in Figures 3(b) and 4(b). It can be seen that the cooling rates after deformation are somewhat larger than before deformation, due to the decreased thickness of the test cell. This is particularly evident for the thermocouple at position B for the larger deformation amount (Figure 4(b)), since it moves considerably closer to the heat exchanger. During deformation, each location experiences a small change or fluctuation in temperature. In both tests, the temperatures at positions 2 and 4

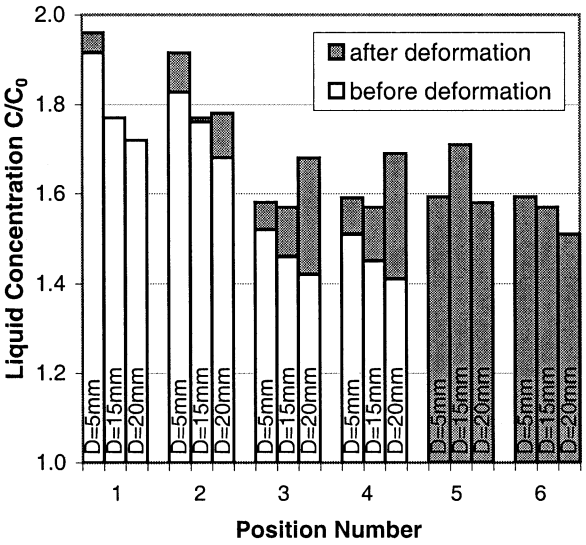

Fig. 5—Effect of the deformation amount, *D*, on the liquid concentrations measured before and after deformation for the same final test cell thickness of 25 mm ($t_S \approx 135$ min, $V = 0.5$ mm/s).

(*i.e.*, at a height of 50 mm) show a slight drop, while the temperatures at positions 1 and 3 (*i.e.*, at a height of 90 mm) increase during deformation. These changes are more pronounced for the larger deformation amount. Before deformation, the thermocouples at positions 5 and 6 (*i.e.*, at a height of 120 mm) are not immersed in the alloy, and no temperatures are plotted. After deformation, these thermocouples are immersed in expelled liquid, in the case of the test with an initial thickness of 30 mm (Figure 3), and in mush, in the case of the test with an initial thickness of 45 mm (Figure 4). This can be inferred from the heights of the upper mush/liquid interfaces after deformation, shown in Figures 2(a) and (c) for the two tests. In Figure 3, the temperatures at positions 5 and 6 are between the temperatures at positions 1/2 and 3/4, indicating that the expelled melt at the top is well mixed and attains some average temperature. On the other hand, in Figure 4, the temperatures at positions 5 and 6 quickly reach the same temperature as at positions 1/2 and 3/4, implying that inside the mush, the temperature gradient does not vary with height, even after deformation.

Figure 5 shows the influence of the amount of deformation on the measured liquid concentrations before and after deformation for the same final test cell thickness of 25 mm in all three cases. The measured liquid concentrations at positions 1 through 4 before deformation correspond to the liquidus concentrations at the local temperatures corresponding to those positions. Consequently, the concentrations are higher at positions 1 and 2 than at 3 and 4, and there is little variation in the vertical direction (*i.e.*, between 1 and 2 as well as between 3 and 4). At each position, the liquid concentration before deformation decreases with increasing initial test-cell thickness (or deformation amount), because the temperatures are generally higher for a larger initial thickness (refer to the discussion of Figures 3 and 4). After deformation, the measured liquid concentrations at positions 2 through 4 increase, while at position 1, they are approximately the same as before deformation. The strong increases in the liquid concentration at positions 3 and 4 (which are located only 2 mm from the fixed phenolic plate after deformation) indicate that solute-rich liquid flows, in response to the deformation, from the colder regions of the mush horizontally toward the fixed phenolic plate. It can be seen that the rise in the liquid concentrations at these positions increases with deformation amount, as expected. Smaller increases are also observed at position 2, indicating that some flow of this nature is also present closer to the heat exchanger. However, the lack of change of the liquid concentration at position 1 implies that the deformation-induced liquid flow in this region is either negligibly small or in an upward direction, parallel to the isotherms. The liquid at position 2 is less likely to flow upward, because of the larger distance to the free surface. The liquid concentrations measured after deformation at positions 5 and 6 reflect the upward flow of liquid due to the deformation. These liquid concentrations are of similar magnitude to those at positions 3 and 4. Most of the upward flow of liquid during deformation can be expected to originate from the lower-solid-fraction, higher-permeability region closer to the fixed phenolic plate. The concentrations at position 5 are somewhat higher than those at position 6, because some liquid from a region closer to the heat exchanger flowed to that location and because the temperature at position 5 is lower than that at position 6. Interestingly, the liquid concentrations at positions 5 and 6 generally decrease with the deformation amount, which is opposite the behavior observed for positions 3 and 4 after deformation (the exception to this trend is seen at position 5 for $D = 5$ mm). This can be explained by the fact that the smaller the initial test cell thickness (and the smaller the deformation amount), the lower the temperature near the fixed phenolic plate is before deformation and, thus, the higher the concentration of the expelled liquid. For the test with $D = 5$ mm, positions 5 and 6 are both located in the expelled liquid, as opposed to in the mush, as in the other tests. They show identical concentrations after deformation because the expelled liquid above the mush/liquid interface is well mixed.

Figures 6(a) through (c) show the measured positions of the two rows of beads embedded in the solid skeleton in the mush for the three different deformation amounts. The positions are measured relative to a coordinate system fixed to the moving heat exchanger on the right-hand side. The arrows drawn between the bead positions before and after deformation show the approximate path of the beads during deformation. Note that the deformation speed (D/t_D) was the same for all three tests (0.5 mm/s). During deformation, it can be seen that the solid in the mush moves not only toward the heat exchanger, but also upward. As expected, the extent of solid displacement increases with distance from the heat exchanger and with the deformation amount. Furthermore, the solid displacements closer to the upper free surface (*i.e.*, at a height of about 90 mm) have a slightly larger upward component than the displacements at a height of about 50 mm.

Further insight into the movement of the solid during deformation can be obtained by focusing on the horizontal displacement of the beads in the thickness direction. Figure 7 plots the final horizontal position of the beads against their initial horizontal position. Linear deformation behavior is indicated as an interrupted line. It is seen from Figures 7(a) through (c) that the measured horizontal solid displacement indeed increases linearly with distance from the heat exchanger. For the larger deformation amounts (Figures 7(b)

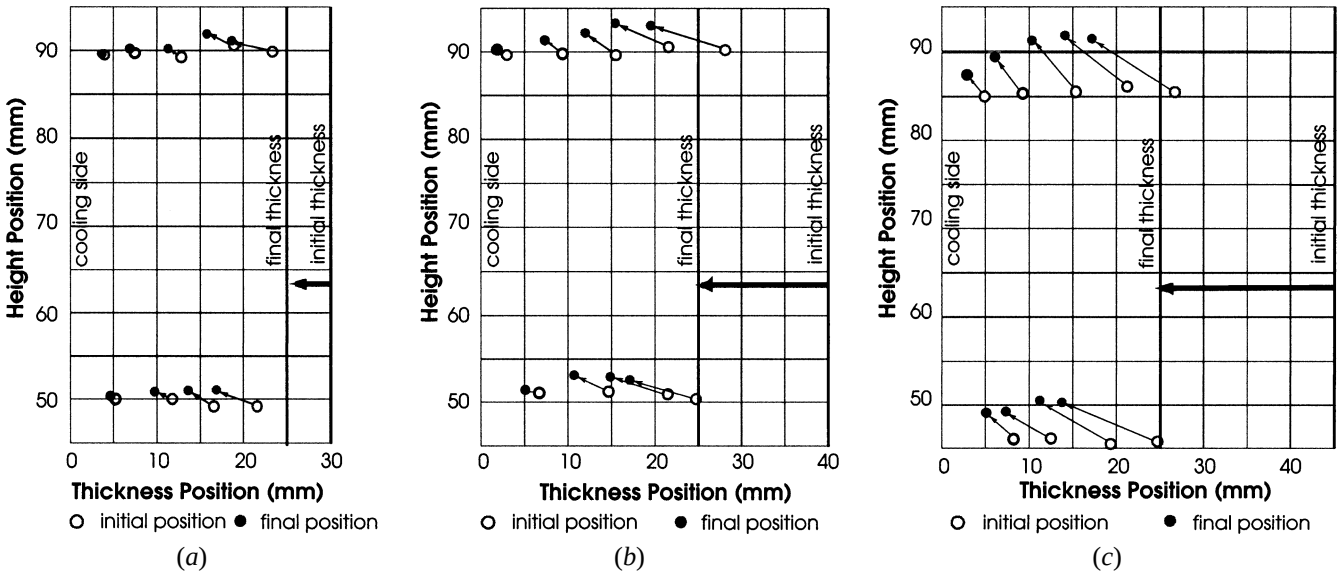

Fig. 6—Positions of the beads embedded in the solid skeleton in the mush measured before and after deformation ($t_S \approx 135$ min, $V = 0.5$ mm/s): (*a*) $L = 30$ mm, $D = 5$ mm; (*b*) $L = 40$ mm, $D = 15$ mm; and (*c*) $L = 45$ mm, $D = 20$ mm.

and (c)), some minor deviation from the ideal behavior represented by the interrupted line is observed.

B. *Influence of Deformation Amount for the Same Initial Thickness*

Additional experiments were conducted to investigate the influence of the amount of deformation for the same initial thickness of the test cell. Recall that in the previous section, the initial thickness was different for each test, which resulted in different conditions before deformation. The initial thickness for the three experiments compared in this section is held constant at 40 mm. The deformation amounts are 5, 10, and 15 mm. The deformation start time (about 135 minutes) and deformation speed (0.5 mm/s) are the same in all three tests.

The measured liquid concentrations before and after deformation are plotted in Figure 8. Before deformation, the liquid concentrations in all three tests are virtually the same, which is expected since the tests have nominally the same conditions before deformation. This comparison, therefore, indicates the repeatability of the measurements. After deformation, the liquid concentrations at position 1 remain approximately the same, as already discussed in connection with Figure 5. At position 2, a slight increase in the concentrations is observed, again in accordance with Figure 5. At positions 3 and 4, the liquid concentrations increase more strongly and the changes increase with deformation amount. Again, these increases can be attributed to the deformation causing solute-rich liquid to flow horizontally from regions closer to the cold heat exchanger toward the fixed phenolic plate. At positions 5 and 6, however, the liquid concentrations increase with deformation amount, which is qualitatively different from the behavior observed in Figure 5. This increase can be explained by the fact that, for the same conditions before deformation, the liquid expelled from the mush has a higher average concentration as the deformation amount is increased.

For completeness, the measured horizontal solid displacements in the thickness direction for the experiments with $D = 5$ and 10 mm are plotted in Figures 9(a) and (b), respectively (the displacements for $D = 15$ mm are already plotted in Figure 7(b)). Again, very linear deformation behavior is observed.

C. *Influence of Initial Thickness for the Same Deformation Amount*

Figure 10 compares two experiments already shown in Figures 5 and 8, where the initial test-cell thickness varies from 30 to 40 mm, while the deformation amount is held constant at 5 mm. The liquid concentrations before deformation are smaller for the larger initial thickness. Since the liquid concentrations in the mush are directly related to the temperatures *via* the liquidus line of the phase diagram, this can be attributed to the temperatures being somewhat higher for the larger initial thickness. The concentration increases at positions 1 through 4 due to deformation are relatively small for both initial thicknesses, since the deformation amount is only 5 mm. For both tests, the liquid concentrations at positions 5 and 6 are the same. As explained earlier, for the deformation amount of 5 mm, positions 5 and 6 are located in the expelled-liquid region above the upper mush/liquid interface (Figure 2(a)), and this liquid is well mixed. The liquid concentrations at positions 5 and 6 are smaller for the larger initial test-cell thickness, which can be attributed to the concentrations in the mush being smaller before deformation.

D. *Influence of Deformation Start Time and Deformation Speed*

Figure 11 shows measured temperatures for a test where the deformation start time was 97 minutes, $L = 30$ mm, and $D = 5$ mm. The plot can be compared directly with Figure 3, where $t_S \approx 135$ minutes and all other conditions are the same. As expected, for an earlier deformation start time, the temperatures just before deformation (Figure 11(b)) are generally higher. Also, the temperature gradient across the

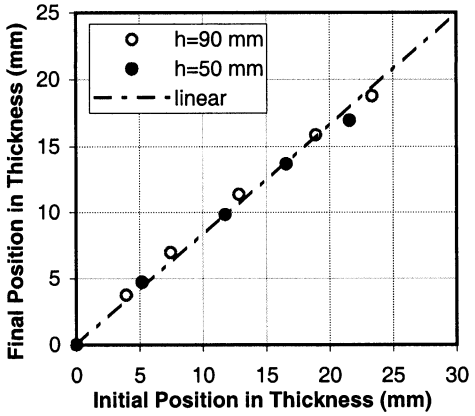

(*a*)

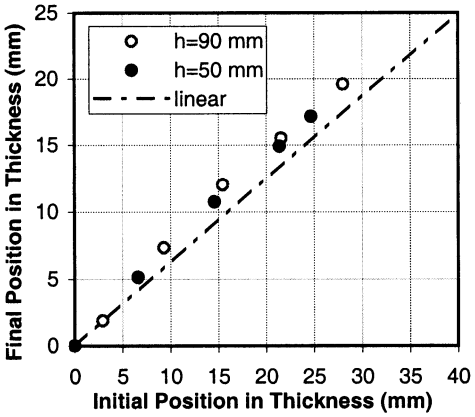

(*b*)

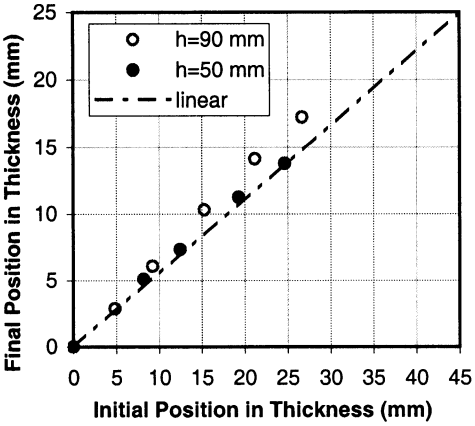

(*c*)

Fig. 7—Horizontal displacement of the beads in the thickness direction before and after deformation ($t_S \approx 135$ min, $V = 0.5$ mm/s): (*a*) $L = 30$ mm, $D = 5$ mm; (*b*) $L = 40$ mm, $D = 15$ mm; and (*c*) $L = 45$ mm, $D = 20$ mm.

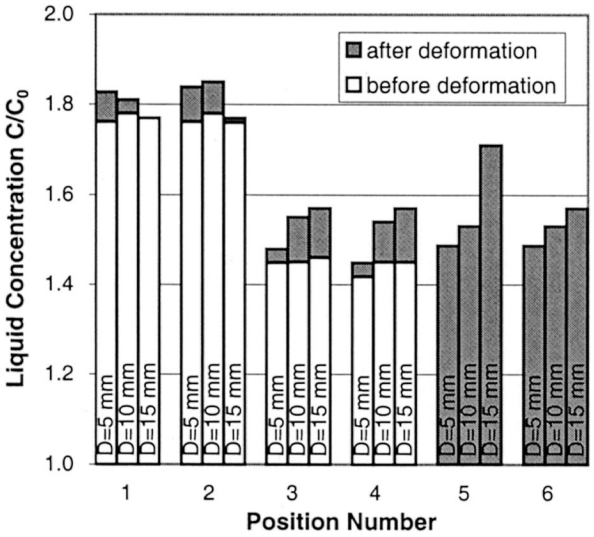

Fig. 8—Effect of the deformation amount, *D*, on the liquid concentrations measured before and after deformation for the same initial test cell thickness of $L = 40$ mm ($t_S \approx 135$ min, $V = 0.5$ mm/s).

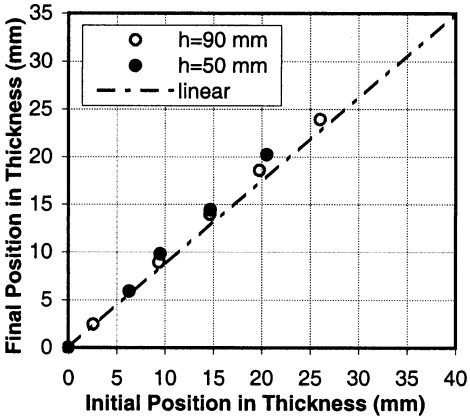

(*a*)

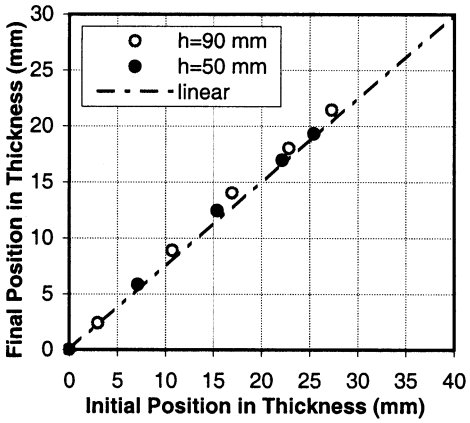

(*b*)

Fig. 9—Horizontal displacement of the beads in the thickness direction before and after deformation ($t_S \approx 135$ min, $V = 0.5$ mm/s): (*a*) $L = 40$ mm, $D = 5$ mm; and (*b*) $L = 40$ mm, $D = 10$ mm.

mush in the thickness direction is higher for an earlier start time. After deformation, the temperatures in Figures 3 and 11 are qualitatively very similar. Although not shown here, the upper liquid-mush interface after deformation is slightly lower for the earlier deformation start time as compared to Figure 2(a). This can be expected for smaller t_S values, because the mush has a lower average solid fraction before deformation.

Figure 12 shows the influence of the deformation start time on the measured liquid concentrations before and after deformation for three different tests with $t_S = 55$, 97, and 135 min. All other conditions are the same ($L = 30$ mm

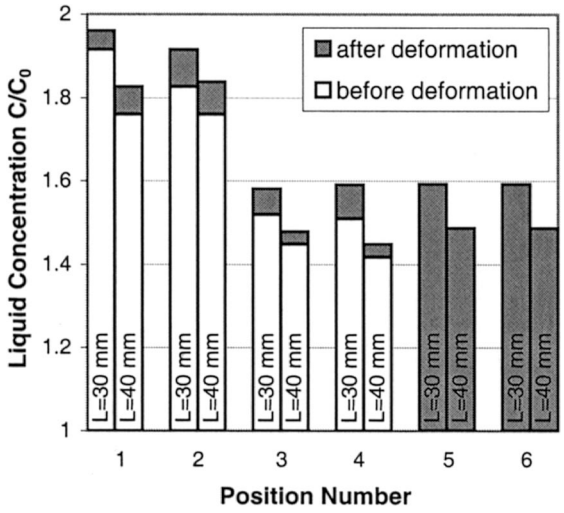

Fig. 10—Effect of the initial test cell thickness, L, on the liquid concentrations measured before and after deformation for the same deformation amount of $D = 5$ mm ($t_S \approx 135$ min, $V = 0.5$ mm/s).

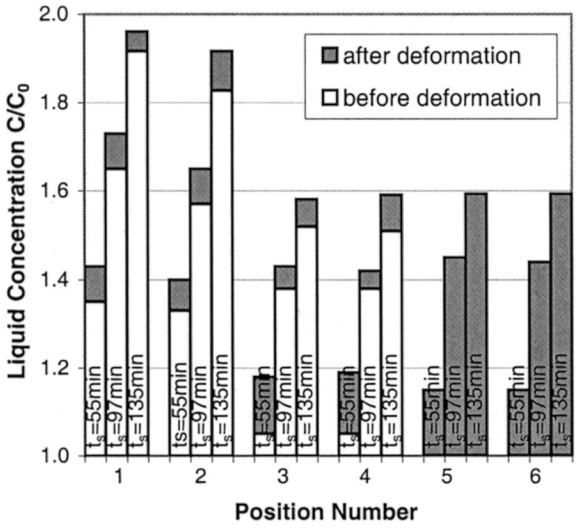

Fig. 12—Effect of the deformation start time, t_S, on the liquid concentrations measured before and after deformation ($L = 30$ mm, $D = 5$ mm, and $V = 0.5$ mm/s).

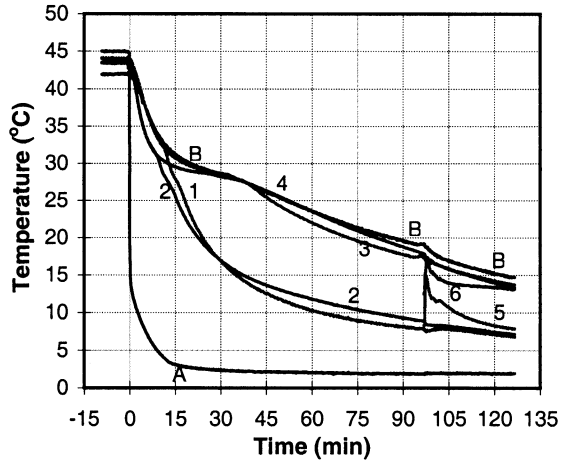

(*a*)

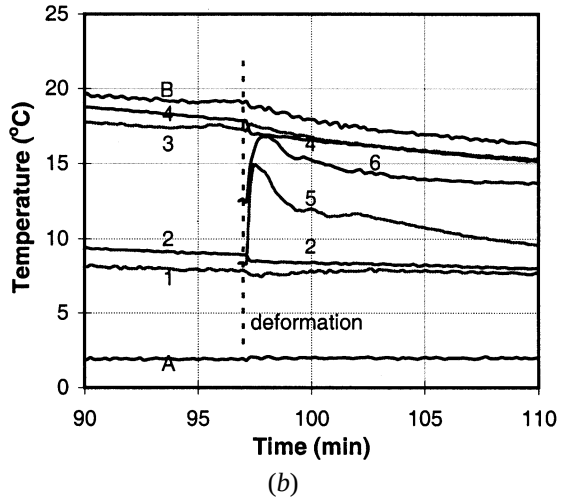

(*b*)

Fig. 11—Temperatures measured during the test with a deformation start time of $t_S = 97$ min ($L = 30$ mm, $D = 5$ mm, and $V = 0.5$ mm/s): (*a*) overall temperature variation and (*b*) close-up of the temperature variation near the deformation time (the vertical dashed line indicates the start of deformation).

and $D = 5$ mm). Before deformation, the concentrations at positions 1 through 4 increase strongly with deformation start time. This is expected, because the temperatures are lower for a later start time, as mentioned previously. In fact, for $t_S = 55$ min, the liquid concentrations at positions 3 and 4 are only slightly above the initial alloy composition C_0, indicating that the temperature near the fixed phenolic plate was only slightly below the liquidus temperature before deformation. The increases in the liquid concentrations at positions 1 through 4 due to deformation are similar in all three tests, which can be expected because the deformation amount was the same. Only the concentration increases at positions 3 and 4 for the test with $t_S = 55$ min are somewhat larger than those for the later deformation start times, which may be attributed to the larger concentration (and temperature) gradients present before deformation. The liquid concentrations at positions 5 and 6 (*i.e.*, in the expelled liquid above the upper mush/liquid interface) increase strongly with deformation start time. This is a direct consequence of the liquid concentrations being higher before deformation for a later deformation start time.

For completeness, the measured horizontal solid displacements in the thickness direction for the experiments with $t_S = 55$ and 97 min are plotted in Figures 13(a) and (b), respectively (the displacements for $t_S = 135$ min are already plotted in Figure 7(a)). As in Figure 7(a), very linear deformation behavior is observed.

Finally, experiments were performed where the duration of the deformation was varied from 10 to 30 seconds, giving deformation speeds between $V = 0.5$ and 0.17 mm/s (with all other conditions the same). No discernable trends were observed in the variations of the measured temperatures, liquid concentrations, or solid displacements with deformation speed. This can probably be attributed to the relatively small range of deformation speeds achievable with the present experimental setup. It is possible that significantly different deformation speeds could influence the transport behaviors during deformation.

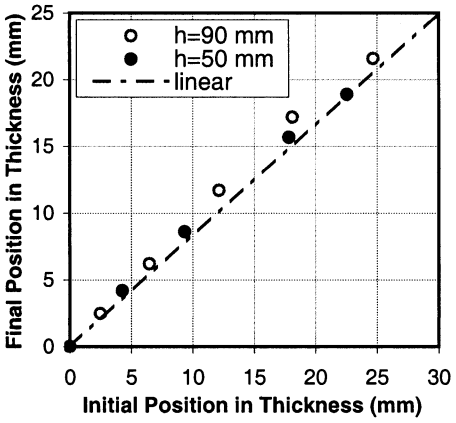

(*a*)

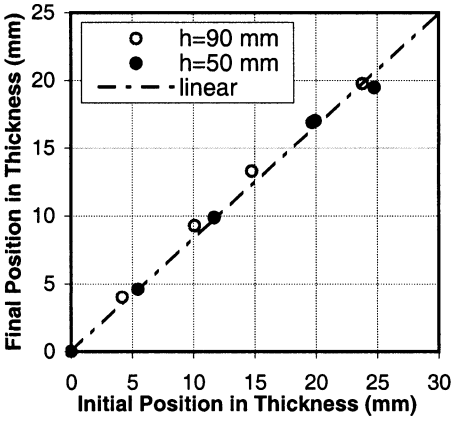

(*b*)

Fig. 13—Horizontal displacement of the beads in the thickness direction before and after deformation (L = 30 mm, D = 5 mm, and V = 0.5 mm/s): (*a*) t_S = 55 min and (*b*) t_S = 97 min.

IV. CONCLUSIONS

A model experiment was developed to study deformation of a directionally solidified columnar dendritic mushy zone, utilizing the transparent alloy SCN-ACE. This alloy not only solidifies like many technologically important metal alloys, but also shows a similar deformation behavior close to the melting point. Its transparency allows for direct observation of the solid growth and deformation behaviors. The experiments were performed in a specially designed test cell which mimics, in some aspects, continuous casting and soft reduction of steel slabs. Deformation is induced by the movement of a cooled side wall (*i.e.*, the heat exchanger) toward a fixed insulating plate representing the centerline in a slab. Measurements include the mush/liquid interface positions, numerous temperatures and liquid concentrations, and the solid displacements at various locations in the mushy zone. These measurements allow for a detailed examination of the solidification behavior and deformation-induced transport phenomena. The relatively simple experimental setup, together with the measurements reported here, should serve well in developing and validating future mathematical models that predict both solid deformation and liquid flow during solidification of alloys. Such models presently do not exist.

The experiments examine the effects of the deformation amount and start time for different initial and final test cell thicknesses. It is found that the deformation induces not only horizontal displacement of the solid skeleton in the mush in the thickness direction, but also upward movement of the solid, as evidenced by the rise of the upper mush/liquid interface. The horizontal solid displacement increases linearly with distance from the heat exchanger. The concentration measurements indicate that liquid is expelled primarily from the higher-permeability region closer to the fixed plate opposing the heat exchanger. The expelled liquid flows upward and accumulates in a layer above the mushy zone. In addition, solute-rich liquid flows horizontally from the heat exchanger toward the fixed plate. Different initial test-cell thicknesses and deformation start times result in different temperatures and, hence, liquid concentrations in the mush before deformation, which, in turn influence the changes in the liquid concentrations due to deformation. Generally, larger deformation amounts cause larger concentration changes. All of the aforementioned effects are quantified by the measurements reported in this article.

Before the present data can be used to validate model predictions, it is necessary to better understand the rheological behavior of a columnar dendritic mush. The present experimental results underline the need for a model in which the solid and liquid phases are allowed to move at different velocities. While such a two-phase model has been developed in principle,[25] a stress-strain relation for the solid-phase momentum equation that accounts for the structure of the solid in the mush is still lacking. Specially designed experiments, where forces are measured, are necessary to develop such a relation.

ACKNOWLEDGMENTS

The authors acknowledge the help of Dr. E.M.S. Rizzo and Mr. V. Raghavendra, both formerly of the University of Iowa, in developing the experimental setup. Partial financial support was provided by NASA under Contract No. NCC8-94.

REFERENCES

1. M. Kawaberi, Y. Yamamoto, and K. Asoh: *Kawasaki Steel Giho*, 1994, vol. 26 (1), pp. 26-32.
2. R. Kopp: *Ann. CIRP*, 1996, vol. 45 (1), pp. 221-25.
3. E. Essadiqi, L.E. Collins, M.T. Shehata, and L.K. Chiang: *2nd Canada-Japan Symp. Modern Steelmaking and Casting Techniques*, J.J. Jonas *et al.*, eds., TMS-CIM, Toronto, 1994, pp. 251-64.
4. S. Ogibayashi, R. Nishihara, and S. Satoh: *Tetsu-to-Hagané*, 1997, vol. 83, pp. 36-41.
5. S. Ogibayashi, M. Kobayshi, M. Yamada, and T. Mukai: *Iron Steel Inst. Jpn. Int.* 1991, vol. 31, pp. 1400-07.
6. S. Thiem and W. Loser: *Steel Res.*, 1992, vol. 63, pp. 291-96.
7. M.C. Flemings and G.E. Nereo: *TMS-AIME*, 1967, vol. 239, pp. 1449-61.
8. K.I. Miyazawa and K. Schwerdtfeger: *Arch. Eisenhüttenwes*, 1981, vol. 52, pp. 415-22.
9. G. Lesoult and S. Sella: *Solid State Phenomena*, 1988, vols. 3–4, pp. 167-78.
10. M. El-Bealy and H. Fredriksson: *Scand. J. Metall.*, 1994, vol. 23, pp. 140-50.
11. T. Kajitani, J.-M. Drezet, and M. Rappaz: *Metall. Mater. Trans. A*, 2001, vol. 32A, pp. 1479-91.
12. H. Kobayashi, S. Kuriyama, T. Masaoka, M. Suzuki, and S. Miyahara: *CAMP-ISIJ*, 1989, vol. 2 (4), pp. 1158-61.
13. S. Ogibayashi, M. Uchimura, K. Isobe, and H. Maede: *CAMP-ISIJ*, 1989, vol. 2 (4), pp. 1162-65.
14. L.K. Chiang: *72nd Steelmaking Conf. Proc.*, Iron and Steel Society, Chicago, IL, 1989, pp. 81-89.

15. T. Fujimura, K. Kushida, and K. Sorimach: *CAMP-ISIJ*, 1989, vol. 2 (4), pp. 1166-69.
16. S. Kojima, H. Mizota, and K. Kushida: *Kawasaki Steel Giho*, 1994, vol. 26 (1), pp. 1-6.
17. H. Bada, F. Sudo and T. Matsukawa: *Kawasaki Steel Giho*, 1994, vol. 26 (1), pp. 13-18.
18. M.E. Glicksman, R.J. Schaefer, and J.D. Ayers: *Metall. Trans. A*, 1976, vol. 7A, pp. 1747-59.
19. M.A. Chopra, M.E. Glicksman, and N.B. Singh: *Metall. Trans. A*, 1988, vol. 19A, pp. 3087-96.
20. D.L. Ceynar and C. Beckermann: *J. Crystal Growth*, 2001, vol. 222, pp. 380-91.
21. O. Prakash and D.R.H. Jones: *Acta Metall. Mater.*, 1992, vol. 40, pp. 3443-49.
22. O. Prakash and D.R.H. Jones: *Acta Mater.*, 1996, vol. 44, pp. 891-97.
23. G.C. Davies and D.R.H. Jones: *Scripta Mater.*, 1996, vol. 35, pp. 523-28.
24. G.C. Davies and D.R.H. Jones: *Acta Mater.*, 1997, vol. 45, pp. 775-89.
25. J. Ni and C. Beckermann: *Metall. Trans. B*, 1991, vol. 22B, pp. 349-61.